A Parameter Identification Problem of Mixed Type Related to the Manufacture of Car Windshields

Philipp Kügler [1]

Abstract

We study the identification of a parameter in a fourth-order elliptic partial differential equation which models the optimal design of car windshields to be manufactured by the sagging process. Considered as second-order equation for the unknown parameter the problem is of mixed type, i.e., changing between elliptic and hyperbolic. Numerical routines for directly solving this equation are not available. In this paper we both theoretically and numerically show that the inverse problem can instead be solved in a stable way by means of a (derivative free) iterative regularization method. Thereby, the course of the iteration nevertheless depends markedly on the mixed type of the second-order equation.

1 Introduction

Forming automotive glass from a flat sheet to a bended car windshield is a challenging field of industrial and academic research. The resulting change in the glass surface area leads to glass deformations that may cause optical distortions of unacceptable refractive and reflective quality. A related problem the manufacturer faces is the limited formability of the glass. Hence, not every shape designed at the drawing table of the car producer can be (immediately) realized in practice such that costly shape corrections may become necessary.

One industrial method favored for the manufacture of car windshields is the sag bending process: A sheet of glass is put over a rigid frame with the desired edge curvature and heated from above. The glass gets viscous and sags under its own weight. The final shape of the glass depends on the viscosity distribution of the glass obtained from varying the temperature. Hence, given a desired target shape, the task is to find the appropriate temperature distribution in order to achieve that goal, see, e.g., [11].

Though the sag bending process operates in the viscous regime, the viscous-elastic analogy allows to consider the Young's modulus E, a spatially varying glass material parameter, to be proportional to the viscosity, see [12]. Then, since the latter is a function of the temperature, see [8], the sag bending process can in a first approximation also be controlled in terms of E, where the bending of the glass sheet is described by means of the

[1]Institut für Industriemathematik, Johannes Kepler Universität, A–4040 Linz, Austria. E-Mail: kuegler@indmath.uni-linz.ac.at.

linear elastic plate theory. Hence, our inverse problem is to identify the parameter E for a given target shape $\hat{w}$, where its solution can finally be used in order to compute the appropriate temperature distribution.

In Section 2, we discuss the fourth order elliptic direct bending problem for which we shall consider two types of boundary conditions concerning the fastening of the glass sheet. In Section 3 we show that the inverse parameter identification problem can be solved by a (recently developed derivative free) iterative regularization method whose convergence can be established under rather natural assumptions. We also discuss the so-called direct approach which leads to a second order partial differential equation of mixed type for the unknown parameter E. Due to the changes between elliptic and hyperbolic regions in dependence on the desired target shape $\hat{w}$, it is an open problem how to directly solve this parameter pde. However, both the convergence rate analysis of the derivative free iterative method and the numerical tests in Section 4 show that this mixed pde-type is reflected in the iterative algorithm. Taking care of this special feature is of independent mathematical interest but also might help to improve existing routines for the control of the sag bending process.

2 The Direct Problem of Bending of a Plate

In a first model based on the viscous-elastic analogy and the linearized elasticity theory, see, e.g., [12], [2] and [8], the sag bending process can be controlled in terms of the Young's modulus E, a spatially varying and positive glass material parameter. Then, the displacements w of the glass sheet are described by the fourth order elliptic partial differential equation

$$\begin{aligned}\frac{t^3}{12(1-\nu^2)}\{(E(w_{xx}+\nu w_{yy}))_{xx}+(E(w_{yy}+\nu w_{xx}))_{yy}&\\ +2(1-\nu)(Ew_{xy})_{xy}\} &= f \text{ in } \Omega, \qquad (2.1)\end{aligned}$$

where t denotes the thickness of the glass plate, $\Omega \subset \mathbb{R}^2$ represents its midplane, $\nu \in (0, 0.5)$ is the glass Poisson ratio and f denotes gravity. As boundary conditions on w we consider either

$$w|_{\partial\Omega} = 0, \quad \frac{\partial w}{\partial n} = 0 \qquad (2.2)$$

for a clamped plate, or

$$w|_{\partial\Omega} = 0, \quad M_n = 0 \text{ on } \partial\Omega \qquad (2.3)$$

for a simply supported plate, i.e., the moment M_n vanishes such that the plate is allowed to freely rotate around the tangent to $\partial\Omega$. In case of a rectangular frame, the second condition in (2.3) simplifies to

$$\begin{aligned} w_{xx}+\nu w_{yy} &= 0 \text{ along the edges with y = constant} \qquad (2.4)\\ w_{yy}+\nu w_{xx} &= 0 \text{ along the edges with x = constant} \qquad (2.5)\end{aligned}$$

due to the positivity of E, see [9]. Already with respect to the inverse problem, where a Hilbert space setup is of advantage for its theoretical and numerical treatment, we next turn to the weak formulation of (2.1). Denoting by Y_0 a closed subspace of the Hilbert space $Y = H^2(\Omega)$ and considering f as an element of the dual space Y_0^*, the displacement $w \in Y_0$ can be sought as the solution of the operator equation

$$A(E)w = f \ \text{ in } \ Y_0^*, \tag{2.6}$$

where $A(E) : Y_0 \to Y_0^*$ is defined via the symmetric bilinear form

$$\begin{aligned} \langle A(E)w, v\rangle \ &= \ \int_\Omega \frac{Et^3}{12(1-\nu^2)} \left[(w_{xx} + w_{yy})(v_{xx} + v_{yy})\right. \\ &\qquad \left. -(1-\nu)(w_{xx}v_{yy} + w_{yy}v_{xx} - 2w_{xy}v_{xy})\right] \, dxdy \end{aligned} \tag{2.7}$$

on $Y_0 \times Y_0$. The space Y_0 is determined by the boundary conditions on w under consideration, where

$$Y_0 = \{w \in Y \,|\, w|_{\partial\Omega} = 0\} \tag{2.8}$$

corresponds to (2.3) and

$$Y_0 = \left\{ w \in Y \,|\, w|_{\partial\Omega} = 0 \wedge \frac{\partial w}{\partial n} = 0 \right\} \tag{2.9}$$

represents (2.2). The next theorem shows that, given an appropriate parameter E, problem (2.6) is uniquely solvable.

Theorem 2.1. *For any Young's modulus E belonging to the set*

$$\tilde{Q} = \left\{ E \in H^1(\Omega) \,|\, \underline{\gamma} \le E \le \bar{\gamma} \right\}, \tag{2.10}$$

where $\underline{\gamma}, \bar{\gamma}$ are positive constants, the direct problem (2.6) *admits a unique solution in Y_0.*

Proof. Simple manipulations of the bilinear form (2.7) yield that the operator $A(E)$ is continuous in the sense

$$|\langle A(E)w, v\rangle| \le \alpha_2 \|w\|\|v\|, \quad w, v \in Y, \ E \in \tilde{Q}, \tag{2.11}$$

with a positive constant $\alpha_2 = \alpha_2(\bar{\gamma})$. Furthermore, since $v \in Y_0$ (both for (2.8) and (2.9)) with v a polynomial of degree one implies $v = 0$, we can apply the theorem on equivalent norms in order to obtain the ellipticity

$$\langle A(E)w, w\rangle \ge \alpha_1 \|w\|^2, \quad w, v \in Y_0, \ E \in \tilde{Q} \tag{2.12}$$

with a positive constant $\alpha_1 = \alpha_1(\underline{\gamma})$. For details we refer to [10]. Hence, by virtue of the Lax-Milgram lemma, see for instance [17], problem (2.6) admits a unique solution in Y_0 for any $E \in \tilde{Q}$. $\square$

In the following we denote the unique solution of (2.6) by w_E in order to emphasize its dependence on the parameter E.

3 The Inverse Problem

Having introduced the direct problem (2.1), (2.6) as a first model for describing the bending of the glass sheet resulting from the sag bending process, we now discuss the associated inverse windshield problem: Given a target shape $\hat{w}$ that satisfies either the boundary condition (2.2) or (2.3), we want to find a positive Young's modulus $E = E(x, y)$ such that the corresponding direct problem admits $\hat{w}$ as its solution.

In this section, we first introduce and analyze a derivative free *iterative* regularization method, then in fact allowing to numerically solve the inverse windshield problem in a stable way. This strategy is based on minimizing the deviation between a computed forward solution of the partial differential equation and the desired target shape. We also focus on the *direct* approach where the idea is to consider the state equation as a second order (partial differential) equation for the unknown parameter. Since this equation then is of mixed type, numerical concepts for its solution are missing. Nevertheless, this approach demands special attention since the mixed type is also reflected in the iterative method.

3.1 The Iterative Approach

Introducing the set of admissible parameters

$$Q = \left\{ E \in X \,|\, \underline{\gamma} \leq E \leq \bar{\gamma} \right\}, \tag{3.13}$$

where X is a Hilbert space, and the parameter-to-output map

$$F : Q \to Y, E \to w_E,$$

where w_E denotes the solution of the direct problem (2.6), the inverse windshield problem can be formulated as the nonlinear operator equation

$$F(E) = \hat{w}. \tag{3.14}$$

In the following, we assume that *the exact data* $\hat{w} \in Y_0$ are attainable by a parameter $E_* \in Q$, i.e., that the windshield is manufacturable. Note that this does not imply that the solution E_* of (3.14) has to be unique. Already translated to the underlying real world problem, several solutions may even be of advantage since they give more freedom in choosing the strategy for heating the glass. Target shapes that would be accepted as well as $\hat{w}$ by the car producer are taken into account as *perturbed data* $w^\delta \in Y_0$, where δ in

$$\|\hat{w} - w^\delta\| \leq \delta \tag{3.15}$$

has to be understood as a level of tolerance for the outcome of the bending process.

Parameter identification problems as (3.14) are typically ill-posed in the sense that their solution does not depend continuously on the data. Hence, data but also round-off errors may be amplified by an arbitrarily large error if one applies methods to (3.14) that are only suited for well-posed problems, see [3]. In order to overcome these instabilities one has to use *regularization* methods. Iterative techniques - especially advantageous for nonlinear problems - are mostly based on a successive minimization of the output least-squares functional

$$E \to \frac{\lambda}{2}\|F(E) - w^\delta\|^2, \tag{3.16}$$

where λ is a scaling parameter, see the survey given in [5]. Though the initial guess E_0 is always supposed to lie in a neighborhood of E_*, i.e.,

$$E_* \in \mathcal{B}_{\rho/2}(E_0), \tag{3.17}$$

where ρ is chosen such that $\mathcal{B}_\rho(E_0) \subset Q$ is satisfied, stability can only be enforced, i.e., a reliable approximation to the solution of (3.14) can only be obtained, if the iteration is stopped at the right time depending on δ. Denoting the iterates by E_k^δ, the discrepancy principle, see for instance [3] or [7], suggests to determine the stopping index $k_*(\delta)$ by

$$\|w^\delta - F(E_{k_*}^\delta)\| \le \tau\delta < \|w^\delta - F(E_k^\delta)\|, \quad 0 \le k < k_*, \tag{3.18}$$

for some sufficiently large $\tau > 0$. The (final) residual $w^\delta - F(E_{k_*}^\delta)$ then is of the order of the tolerance level, which is the best we should ask for.

All the classical iterative regularization methods for solving (3.14), (3.15) in a stable way like the Landweber method

$$E_{k+1}^\delta = E_k^\delta + \lambda F'(E_k^\delta)^*(w^\delta - F(E_k^\delta)), \tag{3.19}$$

see [7], that allow a comprehensive analysis of their convergence behaviour, require the existence of the Fréchet derivative of F and further conditions on F', see [5]. Usually, those are hard to verify for parameter identification problems in higher dimensions. Instead, we apply the *derivative free* Landweber method

$$E_{k+1}^\delta = E_k^\delta + \lambda L(E_k^\delta)^*(w^\delta - w_k), \tag{3.20}$$

introduced in [9], where $L(E)^*$ denotes the Hilbert space adjoint of the linear operator

$$L(E) : X \to Y_0, \ h \to -JA(h)w_E \tag{3.21}$$

for $E \in Q$. Thereby, w_k is used as an abbreviation for $F(E_k^\delta)$, $A(h)$ is defined by (2.7) and $J : Y_0^* \to Y_0$ represents the duality map. For the windshield problem it is of interest to approximate the given target shape also in terms of its second derivatives, since the related curvatures finally characterize the optical quality of the windshield. Hence, it is appropriate to use the full Y-topology in building the adjoint operator of (3.21) (as well as in (3.15)).

In the following, we choose the Hilbert space $X = H^s(\Omega)$ with $s > d/2$ such that $X \subset L^\infty(\Omega)$ is satisfied. Obviously, we have $Q \subset \tilde{Q}$ such that (2.11) and (2.12) especially hold for Q and the forward operator F in fact is well defined. Furthermore, definition (2.7) yields

$$A(\cdot)u \in \mathcal{L}(X, Y_0^*) \tag{3.22}$$

because of

$$\langle A(h)v, w\rangle \leq c\|h\|\|v\|\|w\|, \quad h \in X, v, w \in Y, \tag{3.23}$$

where c denotes the embedding constant. Together with (2.6) and (2.7) this also implies that the iteration operator is locally bounded, i.e.,

$$\|L(E)\| \leq \hat{L}, \quad E \in \mathcal{B}_\rho(E_0) \tag{3.24}$$

with $\hat{L} = c\|f\|/\alpha_1$.

In establishing convergence of the iterates of (3.20) we follow the basic concept of [7]. Since we do not resort to strong conditions on the Fréchet derivative of F, we still have to proceed in a different manner. The first result shows that the error in the parameter is monotonically decreasing as long as the discrepancy principle is obeyed.

Proposition 3.1. *Assume that E_* is a solution of* (3.14) *in $\mathcal{B}_{\rho/2}(E_0)$ and let λ and τ be chosen such that*

$$2\left(\alpha_1 - \frac{\alpha_2}{\tau}\right) - \lambda\hat{L}^2 \geq D \tag{3.25}$$

holds, where D is a fixed positive constant. In case of perturbed data w^δ satisfying (3.15), *we denote by k_* the stopping index of the iteration according to the discrepancy principle* (3.18) *with τ satisfying* (3.25). *Then, we have*

$$\|E_* - E_{k+1}^\delta\| \leq \|E_* - E_k^\delta\|, \quad 0 \leq k < k_*, \tag{3.26}$$

and

$$\sum_{k=0}^{k_*-1} \|w^\delta - w_k\|^2 \leq \frac{\rho^2}{4\lambda D}. \tag{3.27}$$

For $\delta = 0$ (with $\tau = \infty$ in (3.25)*), we have*

$$\sum_{k=0}^{\infty} \|\hat{w} - w_k\|^2 \leq \frac{\rho^2}{4\lambda D}. \tag{3.28}$$

Proof. Given $\|E_0 - E_*\| \le \rho/2$, we assume

$$\|E_k^\delta - E_*\| \le \rho/2$$

for $k < k_*(\delta)$ and argue by induction. Then, the iteration step (3.20) is well-defined, yielding

$$\begin{aligned} & \|E_* - E_{k+1}^\delta\|^2 - \|E_* - E_k^\delta\|^2 \\ = \;& -2\lambda(L(E_k^\delta)(E_* - E_k^\delta), w^\delta - w_k) + \lambda^2\|L(E_k^\delta)^*(w^\delta - w_k)\|^2. \end{aligned} \tag{3.29}$$

The following considerations play the decisive role in our analysis and are only possible for the special iteration operator (3.21). Because of its definition, (3.22) and

$$A(E_*)\hat{w} = A(E_k^\delta)w_k \;\text{ in }\; Y_0^*,$$

we get

$$\begin{aligned} & -(w^\delta - w_k, L(E_k^\delta)(E_* - E_k^\delta)) \\ = \;& \langle w^\delta - w_k, A(E_* - E_k^\delta)w_k\rangle \\ = \;& \langle w^\delta - w_k, A(E_*)w_k - A(E_*)\hat{w}\rangle \\ = \;& -\langle w^\delta - w_k, A(E_*)w^\delta - A(E_*)w_k\rangle + \langle w^\delta - w_k, A(E_*)w^\delta - A(E_*)\hat{w}\rangle \\ \le \;& -\alpha_1\|w^\delta - w_k\|^2 + \alpha_2\|w^\delta - w_k\|\|w^\delta - \hat{w}\|, \end{aligned} \tag{3.30}$$

where the inequality holds because of (2.12) and (2.11). Using (3.30) in (3.29), we obtain

$$\begin{aligned} & \|E_* - E_{k+1}^\delta\|^2 - \|E_* - E_k^\delta\|^2 \\ \le \;& \|w^\delta - w_k\|\lambda\left(2\alpha_2\delta - 2\alpha_1\|w^\delta - w_k\| + \lambda\hat{L}^2\|w^\delta - w_k\|\right). \end{aligned}$$

Following the discrepancy principle (3.18), we get from (3.25) that

$$\|E_* - E_{k+1}^\delta\|^2 + \lambda D\|w^\delta - w_k\|^2 \le \|E_* - E_k^\delta\|^2$$

for $k < k_* = k_*(\delta)$. This implies assertion (3.26) and $E_{k+1}^\delta \in \mathcal{B}_{\rho/2}(E_*) \subset \mathcal{B}_\rho(E_0)$. Furthermore, we can conclude that

$$\lambda D\sum_{k=0}^{k_*-1}\|w^\delta - w_k\|^2 \le \sum_{k=0}^{k_*-1}\left(\|E_k^\delta - E_*\|^2 - \|E_{k+1}^\delta - E_*\|^2\right)$$

holds, which leads to the inequality

$$k_*\tau^2\delta^2 \le \sum_{k=0}^{k_*-1}\|w^\delta - w_k\|^2 \le \frac{\rho^2}{4\lambda D}$$

and finally to assertion (3.28). $\square$

Hence, the monotonicity of the iterates, which is the fundament for the forthcoming convergence results, can be guaranteed under natural assumptions already associated to the solvability of the direct problem. Regarding condition (3.25) we see that it can always be satisfied by choosing the λ sufficiently small and τ sufficiently large. Note that - in case of perturbed data - the use of a "large" τ in the discrepancy principle (3.18) might cause a too early termination of the iteration, a problem that is also present when using other iterative methods as, e.g., (3.19). However, our choice of τ in (3.25) no longer involves (in practical situations) unknown constants that are linked to conditions on F', compare to [7].

The estimation (3.28) shows that in the absence of data noise the residual norms of the iterates tend to zero for $k \to \infty$, hence - if the iteration converges - the limit certainly is a solution of the inverse windshield problem. In the case of perturbed data, (3.27) yields the existence of a unique stopping index k_* such that $\|w^\delta - w_k\| > \tau\delta$ holds for all $k < k_*$, but is violated at $k = k_*$.

The next theorem shows that for precise data, the iterates E_k in fact converge to a solution of the inverse windshield problem. Furthermore, in the presence of data perturbations, the discrepancy principle (3.18) renders the derivative free Landweber iteration (3.20) a regularization method, i.e., we have $E^\delta_{k_*(\delta)} \to E_*$ as $\delta \to 0$.

Theorem 3.1 (Convergence). *Let* $\delta = 0$ *in* (3.15). *If* (3.14) *is solvable in* $\mathcal{B}_{\rho/2}(E_0)$, *then* E_k *converges to a solution* $E_* \in \mathcal{B}_{\rho/2}(E_0)$ *of* (3.14), *i.e,*

$$E_k \to E_*, \quad k \to \infty \tag{3.31}$$

In case of perturbed data w^δ *satisfying* (3.15), *let the iteration* (3.20) *be stopped at* $k_*(\delta)$, *according to the discrepancy principle* (3.18), (3.25). *Then*

$$E^\delta_{k_*(\delta)} \to E_*, \quad \delta \to 0. \tag{3.32}$$

Proof. Again we can follow [7], but once more only require the properties of the pde-operator $A(E)$. For exact data, the basic idea is to verify that E_k is a Cauchy sequence. If $\tilde{E}$ denotes any solution of (3.14) in $\mathcal{B}_{\rho/2}(E_0)$, i.e., $w_{\tilde{E}} = \hat{w}$, the crucial ingredient for the proof is

$$\begin{aligned}
(\hat{w} - w_r, L(E_r)(\tilde{E} - E_l)) &= -\langle A(\tilde{E} - E_l)w_r, \hat{w} - w_r\rangle \\
&= -\langle A(\tilde{E} - E_r)w_r, \hat{w} - w_r\rangle \\
&\quad -\langle A(E_r - E_l)w_r, \hat{w} - w_r\rangle \\
&= \langle A(\tilde{E})\hat{w} - A(\tilde{E})w_r, \hat{w} - w_r\rangle \\
&\quad -\langle A(E_l)w_l - A(E_l)w_r, \hat{w} - w_r\rangle, \qquad (3.33)
\end{aligned}$$

which holds because of (3.21), (3.22) and

$$
\begin{aligned}
A(E_r)w_r &= A(\tilde{E})\hat{w} \text{ in } Y_0^*, \\
A(E_r)w_r &= A(E_l)w_l \text{ in } Y_0^*.
\end{aligned}
$$

Given (3.33), one can show as in [7] that $E_k - \tilde{E}$ and hence E_k are Cauchy sequences. Denoting the limit of E_k by E_* we obtain that E_* is a solution of (3.14) since the residues $\hat{w} - w_k$ converge to zero for $k \to \infty$, see Proposition 3.1.

In case of perturbed data, the proof given in [7] is independent of the iteration operator and therefore also applies to (3.20). $\square$

Hence, the derivative free iteration (3.20) in combination with (3.18) provides a numerically stable algorithm for solving the inverse windshield problem. In order to make it more transparent, we build the inner product in X of both sides with a test function $h \in X$. Using (3.21) and rearranging the terms then yields

$$
\begin{aligned}
(E_{k+1}^\delta - E_k^\delta, h) &= -\lambda \frac{t^3}{12(1-\nu^2)} \left\{ \int_\Omega h(w_{kxx}(w^\delta - w_k)_{xx} + w_{kyy}(w^\delta - w_k)_{yy}) dxdy \right. \\
&\quad + \int_\Omega \nu h(w_{kxx}(w^\delta - w_k)_{yy} + w_{kyy}(w^\delta - w_k)_{xx}) dxdy \\
&\quad \left. + \int_\Omega 2(1-\nu) h w_{kxy}(w^\delta - w_k)_{xy} dxdy \right\}. \qquad (3.34)
\end{aligned}
$$

As opposed to (3.19), where $F'(E_k^\delta)^*$ also requires to solve (2.6) with f replaced by the current residual $w^\delta - F(E_k^\delta)$, (3.20) only calls for the computation of w_k. In that sense, the total number of "direct problems" to be solved is cut into halves by (3.20).

3.2 The Direct Approach

Given a target shape $\hat{w}$, one also might look for a solution of the inverse problem by considering (2.1) as a partial differential equation for E, i.e.,

$$
((\hat{w}_{xx} + \nu \hat{w}_{yy})E)_{xx} + 2(1-\nu)(\hat{w}_{xy}E)_{xy} + ((\hat{w}_{yy} + \nu \hat{w}_{xx})E)_{yy} = \frac{12(1-\nu^2)}{t^3} f \text{ in } \Omega. \qquad (3.35)
$$

Usually, parameter identification problems are, when regarded as equations for the unknown parameter, of first order, i.e., the parameter appears at most up to its first derivatives. However, we now face an inverse problem that is of second order in the parameter. The type of equation (3.35) depends on the sign of

$$
\bar{\Delta} = (\hat{w}_{xx} + \nu \hat{w}_{yy}) \cdot (\hat{w}_{yy} + \nu \hat{w}_{xx}) - (1-\nu)^2 \hat{w}_{xy}^2 : \qquad (3.36)
$$

equation (3.35) is elliptic where $\bar{\Delta} > 0$ and hyperbolic where $\bar{\Delta} < 0$. Note that the type depends in fact on the given target shape $\hat{w}$. The discriminant $\bar{\Delta}$ can also be written as

$$\bar{\Delta} = 4\nu(\frac{\hat{w}_{xx} + \hat{w}_{yy}}{2})^2 + (1-\nu)^2(\hat{w}_{xx}\hat{w}_{yy} - \hat{w}_{xy}^2), \tag{3.37}$$

where

$$C_G = \hat{w}_{xx}\hat{w}_{yy} - \hat{w}_{xy}^2$$

is the Gaussian curvature and

$$C_m = \frac{1}{2}(\hat{w}_{xx} + \hat{w}_{yy})$$

is the mean curvature of the shape.

Concentrating on rectangular frames - practice exposes them as the most problematic ones for the sag bending process - we next follow [16] in order to demonstrate that the direct approach for the inverse windshield problem leads to partial differential equations that are always of mixed type. Furthermore, we will see that there is a significant difference in the type between shapes satisfying (2.2) and those fulfilling (2.3).

In the simply supported case (2.3), (2.4), (2.5) and the positivity of E imply that the product of $(\hat{w}_{xx} + \nu\hat{w}_{yy})$ and $(\hat{w}_{yy} + \nu\hat{w}_{xx})$ in (3.36) is zero on any simply supported edge. Hence, $\bar{\Delta} \leq 0$ holds on the edges and equation (3.35) gets hyperbolic or parabolic there.

On the other hand, windshields usually have a positive Gaussian curvature C_G in their interior, i.e., choosing an interior point, its neighbourhood only lies on one side of the tangential plane. Then, (3.37) shows that $\bar{\Delta} > 0$ such that the parameter equation (3.35) is elliptic in these regions. As a consequence, the equation type changes from hyperbolic near to the edges to elliptic near to the centre of the region. Furthermore, It is shown in [16] that there is only one parabolic curve, i.e., a line defined by the points satisfying $\bar{\Delta} = 0$, and that it intersects each of the four sides of the squared frame at a single point. Hence, equation (3.35) is elliptic in the centre and hyperbolic next to the corners of the frame. This typical behaviour is illustrated in Figure 1.

Also in the clamped case (2.2), the equation for E will be elliptic in the centre region according to the positive Gaussian curvature C_G of the target shape. However, along the edges of the frame, the situation is significantly different. For a rectangular frame, the zero gradient condition on the boundary turns to $w_x = 0$ and $w_y = 0$ on the edges $x = const.$ and $y = const.$, respectively. Concentrating on a single edge, e.g., $x = const.$, and differentiating $w_x = 0$ as well as the zero deflection condition $w = 0$ with respect to y, we obtain that also w_y, w_{yy} and w_{xy} vanish along that edge. But then, the discriminant $\bar{\Delta}$, see (3.37), there reduces to

$$\bar{\Delta}_{x=const.} = \nu w_{xx}^2,$$

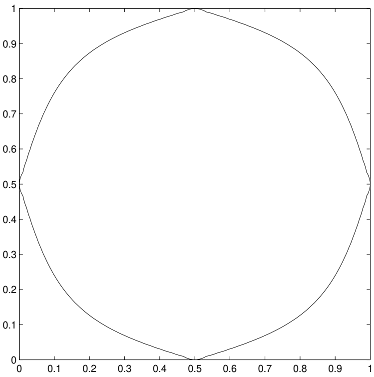

Figure 1: The simply supported case: an elliptic centre area with adjacent hyperbolic corners

such that equation (3.35) cannot be hyperbolic along that edge. In fact, since w_{xx} vanishes only at the ends of the edge $x = const.$, the equation is elliptic along the edge and parabolic only at the very corners. Nevertheless, it is shown in [16] that the elliptic regions near to the frame and in the centre are divided by a hyperbolic ring. Opposed to the simply supported case, there now exist two distinct parabolic lines, where the outer one does not touch the edges of the domain Ω at all. A typical formation of the elliptic and hyperbolic regions is shown in Figure 2.

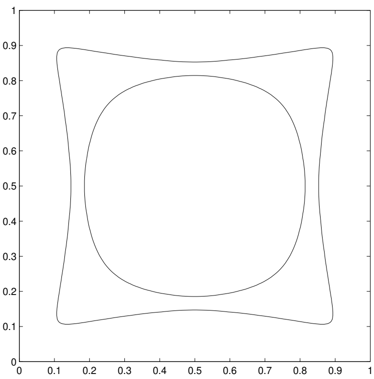

Figure 2: The clamped case: a hyperbolic ring between two elliptic areas

Facing a second order partial differential equation of mixed type, questions concerning existence, uniqueness and stability of a solution to (3.35) arise. Naturally, one would call for boundary conditions for E on $\partial\Omega$ in case of a purely elliptic equation ($\bar{\Delta} > 0$ on Ω) and for Cauchy data on a suitable (non-characteristic) part $\Gamma \subset \partial\Omega$ in a purely hyperbolic case ($\bar{\Delta} < 0$ on Ω). But for the present problem (3.35) with $\hat{w}$ satisfying (2.2) or (2.3), it is not at all obvious how to proceed. The study in [16] of the characteristics of (3.35), where the two characteristic directions are given by

$$\frac{dy}{dx} = \frac{(1-\nu)\hat{w}_{xy} \pm \sqrt{(1-\nu)^2\hat{w}_{xy}^2 - (\hat{w}_{xx} + \nu\hat{w}_{yy}) \cdot (\hat{w}_{yy} + \nu\hat{w}_{xx})}}{\hat{w}_{xx} + \nu\hat{w}_{yy}},$$

see [13], gave some additional insight - for instance, though equation (3.35) is hyperbolic near to the corners of the frame in the simply supported case, one cannot prescribe Cauchy data due to the fact that the edges are characteristics. However, it is not even clear if side conditions on E should be prescribed at all.

So far, results about existence, uniqueness or stability with respect to the data $\hat{w}$ of a solution to problem (3.35) are only available for special symmetric cases, see [14]. Since especially numerical techniques for solving the equation of mixed type are missing, the direct approach (at the moment) is not suited for solving the inverse windshield problem. Nevertheless, returning to our iterative approach (3.20), we shall see that the features of the direct one must not be neglected.

3.3 A First Theoretical Link

In general, the convergence in (3.31), (3.32) for iterative regularization methods may be arbitrarily slow, see [15]. Rate estimates can only be obtained under additional assumptions on the quality of the initial guess E_0 that are often difficult to comprehend, see [5]. Enhancing (3.20) by an additionally stabilizing term, i.e., considering

$$E_{k+1}^\delta = E_k^\delta + L(E_k^\delta)^*(w^\delta - w_k) - \beta_k(E_k^\delta - E_0)$$

with a certain non-negative sequence of decaying parameters β_k, the convergence rates

$$\begin{aligned} \|E_k - E_*\| &= \mathcal{O}(\sqrt{\beta_k}) \qquad \text{(for exact data), and} \\ \|E_{k_*(\delta)}^\delta - E_*\| &= \mathcal{O}(\sqrt{\beta_{k_*(\delta)}}) \end{aligned}$$

could be proven in [9] under the so-called *weak source condition*

$$\exists u \in Y_0 \quad E_* - E_0 = L(E_*)^* u. \tag{3.38}$$

In order to gain more insight into (3.38), we use the definition of $L(E_*)$ and multiply both sides by an arbitrary element $h \in X$. Then, condition (3.38) assumes the existence of a source function $u \in Y_0$ such that

$$\begin{aligned} \frac{12(1-\nu^2)}{t^3}(E_* - E_0, h) &= -\int_\Omega h(\hat{w}_{xx}u_{xx} + \hat{w}_{yy}u_{yy})dxdy \\ &\quad -\int_\Omega \nu h(\hat{w}_{xx}u_{yy} + \hat{w}_{yy}u_{xx})dxdy \\ &\quad -2\int_\Omega (1-\nu)h\hat{w}_{xy}u_{xy}d\vec{x} \end{aligned}$$

holds. If $E_* - E_0$ is sufficiently smooth and if the boundary values of the initial guess E_0 coincide with those of E_*, we obtain

$$(E_* - E_0, h) = \int_\Omega N_X^* N_X (E_* - E_0) \cdot h \, dx, \tag{3.39}$$

where N_X denotes the linear operator that generates the norm in X, e.g., $N_X^* N_X = (I - \Delta - \Delta^2)$ for $X = H^2(\Omega)$. Hence, the weak source condition can be understood as a solvability condition for the second order differential equation

$$\begin{aligned} -\frac{12(1-\nu^2)}{t^3} N_X^* N_X (E_* - E_0) &= (\hat{w}_{xx} u_{xx} + \hat{w}_{yy} u_{yy}) \\ &\quad + \nu(\hat{w}_{xx} u_{yy} + \hat{w}_{yy} u_{xx}) \\ &\quad + 2(1-\nu)\hat{w}_{xy} u_{xy} \end{aligned}$$

for the unknown function $u \in Y_0$. Rearranging the terms on the right-hand side, we end up with

$$\begin{aligned} -\frac{12(1-\nu^2)}{t^3} N_X^* N_X (E_* - E_0) &= (\hat{w}_{xx} + \nu \hat{w}_{yy}) u_{xx} + (\hat{w}_{yy} + \nu \hat{w}_{xx}) u_{yy} \\ &\quad + 2(1-\nu)\hat{w}_{xy} u_{xy}. \end{aligned} \tag{3.40}$$

Now, building the discriminant of (3.40) shows that the type of equation (3.40) is identical to that of the second order partial differential equation (3.35) for E.

Though we assume the attainability of the target shape $\hat{w}$, which can in fact be understood as a solvability assumption for the parameter equation (3.35), this does not automatically imply the solvability of (3.40), since lower order terms in the unknown function are missing in the latter. We also mention that the boundary conditions for a possible solution of (3.40) are already determined by the space Y_0. Since both (2.2) and (2.3) are natural boundary conditions for a fourth order equation, they might be inappropriate for (3.40).

Nevertheless, (3.40) gives a first theoretical coupling between the direct and the iterative approach to solve the inverse windshield problem. The next section shows that the inverse problem can be practically solved by our iterative method (3.20), but also numerically confirms the influence of the mixed type of (3.35) on the course of the iteration. We emphasize that the relation between the parameter pde and the iterative regularization method is neither specific to the windshield problem nor to method (3.20). We refer to [4], where the classical Landweber iteration (3.19) was applied to a second order parameter identification problem with a type ranging from purely hyperbolic to purely elliptic in dependence on the given target.

4 Numerical Experiments

4.1 Preliminaries

Though the windshield problem only yields strictly mixed type equations (3.35), still the significant difference between the simply supported and the hyperbolic situation allows to both test the iterative method and to numerically investigate the influence of the equation type on its outcome. For that purpose, neither the thickness t of the plate, the right-hand side f, the Poisson ratio ν nor the scaling of the parameter E are of relevance. With $\nu = 0.5$, the direct problem (2.6) then turns into

$$\begin{aligned} &\int_\Omega E\left[(w_{xx}+w_{yy})(v_{xx}+v_{yy})\right. && (4.41)\\ -\frac{1}{2}(w_{xx}v_{yy}+w_{yy}v_{xx}&\left.-2w_{xy}v_{xy})\right]\,dxdy \;=\; \int_\Omega \tilde{f}v\,dxdy \quad v\in Y_0, \end{aligned}$$

with the solution space either given by (2.8) or (2.9). The use of a non-physical right-hand side $\tilde{f}$, i.e., not representing the gravity force, facilitates the construction of test examples for which the solution of the inverse problem is analytically known.

Though the convergence analysis of (3.20) - and of the methods discussed in [5] - applied to the windshield problem would require a parameter space satisfying $X \subset L^\infty(\Omega)$, see (3.13), we choose $X = H^1(\Omega)$ for the numerics. On the one hand, this allows to keep the numerical efforts low (since the use of higher order elements for the parameter is avoided), on the other hand it responds to the natural wish for keeping the regularity that is sufficient for the direct problem, compare to (2.10). All our tests have shown that the iterates remain in the domain $\tilde{Q}$ of the parameter-to-output map F without the use of a projection operator.

As a last small deviation from the theoretical fundament, we shall use a line search algorithm, see [6], in order to accelerate (3.20). This results in an iteration index dependent "scaling" parameter λ_k (compared to a constant λ as required by the theory, this has no other influence on the course of the iteration than speeding it up, see [9]), i.e., the iterations finally reads as

$$E^\delta_{k+1} = E^\delta_k + \lambda_k \bar{E}_k, \tag{4.42}$$

where *the update* $\bar{E}_k$ satisfies

$$\begin{aligned} (\bar{E}_k, h) \;=\; -\int_\Omega h\,\big\{&(w_{kxx}(w^\delta - w_k)_{xx} + w_{kyy}(w^\delta - w_k)_{yy}) && (4.43)\\ &+\frac{1}{2}(w_{kxx}(w^\delta - w_k)_{yy} + w_{kyy}(w^\delta - w_k)_{xx})\\ &+w_{kxy}(w^\delta - w_k)_{xy}\big\}\,dxdy, \end{aligned}$$

compare to (3.34). Due to the choice $X = H^1(\Omega)$, equation (4.43) can be considered as the weak formulation of

$$\begin{aligned} \bar{E}_k - \Delta \bar{E}_k &= -\big\{(w_{kxx}(w^\delta - w_k)_{xx} + w_{kyy}(w^\delta - w_k)_{yy}) \\ &\qquad + \frac{1}{2}(w_{kxx}(w^\delta - w_k)_{yy} + w_{kyy}(w^\delta - w_k)_{xx}) \\ &\qquad + w_{kxy}(w^\delta - w_k)_{xy}\big\} \ \text{ in } \Omega, \end{aligned} \tag{4.44}$$

$$\frac{\partial \bar{E}_k}{\partial n} = 0 \ \text{ on } \partial\Omega. \tag{4.45}$$

Hence, one iteration step in order to solve the inverse windshield problem consists of:

1. Given E_k^δ, calculate the solution w_k of the direct problem.
2. Build the residual $w^\delta - w_k$ and solve problem (4.44), (4.45) for the update $\bar{E}_k$.
3. Then, the new iterate E_{k+1}^δ is given by (4.42).

We emphasize that the second order partial differential equation (4.44) for $\bar{E}_k$ is purely elliptic, hence the iterative algorithm never requires to solve the second order equation (3.35) for the parameter such that there is no obvious connection to the mixed type resulting from the direct approach. The boundary condition (4.45) shows that the boundary flux $\frac{\partial E_0}{\partial n}$ of the initial guess E_0 is maintained during the whole iteration.

All computations to be presented in the following are based on the PDE Toolbox of MATLAB, using the finite element method. For the parameter we chose the built-in linear ansatz functions, while the solutions of the direct problem were represented by means of the discrete Kirchhoff triangle, see [1]. Furthermore, a regular and uniform triangular mesh with 665 nodes was used for $\Omega = [0,1] \times [0,1]$.

4.2 Simply Supported vs. Clamped Target Shape

For the numerical test we consider a clamped target shape

$$\hat{w}_C = -25(x^2 - 2x^3 + x^4)(y^2 - 2y^3 + y^4), \tag{4.46}$$

a simply supported target shape

$$\hat{w}_S = -(x - 2x^3 + x^4)(y - 2y^3 + y^4) \tag{4.47}$$

and a true parameter

$$E_* = 1 + x + 2y \tag{4.48}$$

on the unit square. The right-hand side $\tilde{f}$ in (4.41) is chosen such that $F(E_*) = \hat{w}_C$ or $F(E_*) = \hat{w}_S$ holds, respectively. Though we treat in fact two different direct problems, one for the simply supported and one for the clamped plate, this is no barrier for testing our algorithm and for comparing the respective inverse problems with respect to the parameter pde structure. The elliptic and hyperbolic regions of (3.35) corresponding to $\hat{w}_S$ and $\hat{w}_C$ are those shown in Figures 1 and 2.

Ignoring data perturbations for the moment, we choose

$$E_0 = 4 \tag{4.49}$$

as initial guess, meaning a relative deviation from E_* of approximately 80% measured with respect to the norm in X. The course of the iterations is documented in Figures 3 and 4, where the relative error

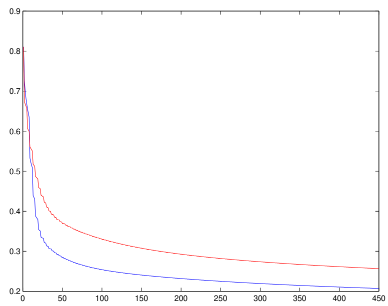

Figure 3: (4.50) vs. k

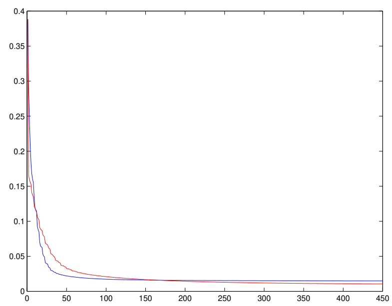

Figure 4: (4.51) vs. k

$$\frac{||E_* - E_k||}{||E_*||} \tag{4.50}$$

in the parameter, but also the relative error in the output, i.e.,

$$\frac{||\hat{w} - w_k||}{||\hat{w}||} \tag{4.51}$$

is plotted vs. the iteration index (the relative error in the $L^2(\Omega)$-norm is approx. tenth part of that shown). The simply supported case is represented by the red line, the clamped case by the blue one. Figure 4 shows that the simply supported and the clamped target shape are approximated with nearly the same quality by our method. The relative error is smaller than 2%, which is remarkable since the deviation in (4.51) is measured with respect to $H^2(\Omega)$. Regarding the relative error in the parameter, we observe a first difference between the simply supported and the clamped situation. Starting both computations from (4.49), it is an open question why the "clamped" error is significantly lower than the "simply supported" one.

Figures 5 and 6 confirm the quality of the computed outputs, while the corresponding

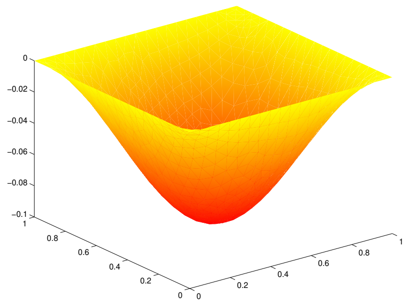

Figure 5: computed output w_{450}, simply supported

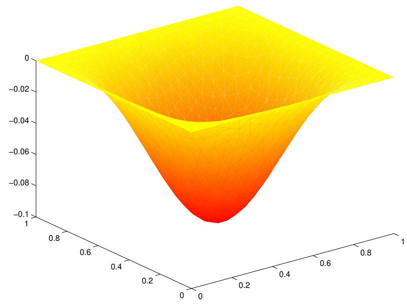

Figure 6: computed output w_{450}, clamped

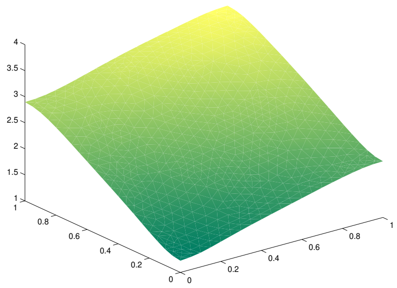

Figure 7: E_{450}, simply supported example

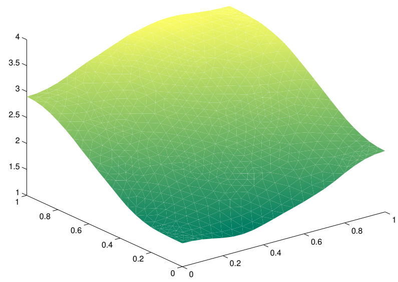

Figure 8: E_{450}, clamped example

parameters E_{450} are shown in Figures 7 and 8. In fact, the total $L^2(\Omega)$-deviations between E_* and E_{450} are nearly identical, while the total deviations in the gradient are higher in the simply supported case than in the clamped one. The oscillations along the boundary $\partial\Omega$ in both cases are caused by the pursuit of satisfying the boundary condition

$$\frac{\partial E_k}{\partial n} = 0$$

due to the initial guess (4.49), compare to (4.45).

Not knowing the boundary values of the solution E_* (as in the previous example) one might think of an iteration procedure that ignores them at all. For that purpose we could only use the $L^2(\Omega)$-inner product in the left-hand side of (4.43), then resulting in the update rule

$$\begin{aligned} \bar{E}_k \quad = \quad & -\big\{(w_{kxx}(w^\delta - w_k)_{xx} + w_{kyy}(w^\delta - w_k)_{yy}) \\ & +\frac{1}{2}(w_{kxx}(w^\delta - w_k)_{yy} + w_{kyy}(w^\delta - w_k)_{xx}) \\ & +w_{kxy}(w^\delta - w_k)_{xy}\big\} \quad \text{in} \quad \Omega. \end{aligned} \tag{4.52}$$

Algorithm (4.52) can be related to the abstract formulation (3.20) by building the adjoint of the iteration operator $L(E_k^\delta)$ only with respect to the rougher space $L^2(\Omega)$. As opposed to (4.44), (4.52) does not describe a boundary value problem for the update $\bar{E}_k$. Though the parameters are still considered as elements belonging to $H^1(\Omega)$, boundary traces of the initial guess are no more maintained during the iteration (at least not in an obvious way). Figures 9 and 10 show the performance of the iteration when using only the update

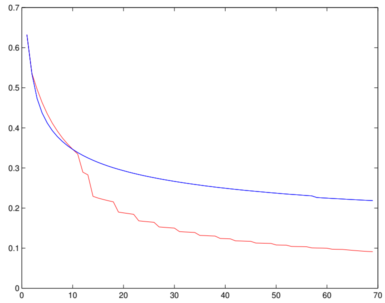

Figure 9: (4.53) vs. k, simply supported vs. clamped

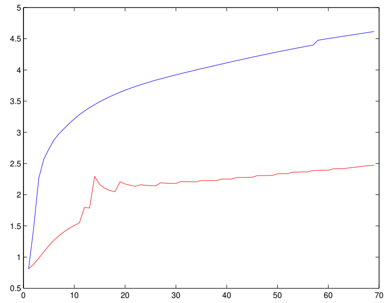

Figure 10: (4.50) vs. k, simply supported vs. clamped

rule (4.52), where the relative error

$$\frac{||E_* - E_k||_{L^2(\Omega)}}{||E_*||_{L^2(\Omega)}} \tag{4.53}$$

vs. k is plotted in Figure 9, while the error (4.50) with respect to $H^1(\Omega)$ is recorded in Figure 10. Concerning the outputs w_k, the error behaviour is similar to that shown in Figure 4, hence we only concentrate on the parameters E_k. The $L^2(\Omega)$-error in the simply supported situation (red line) now lies below its clamped counterpart (blue line) - a ranking opposed to that shown in Figure 3. Regarding the $H^1(\Omega)$-norm, the iteration shows a divergent behaviour, i.e., the error increases from the very beginning, leading to highly oscillating parameters as illustrated in Figures 11 and 12. Thereby, dark green means small errors while light green represents large deviations from the true parameter. Regarding the computed solutions from the top, see Figures 13 and 14, a comparison to the elliptic and hyperbolic regions, see Figures 1 and 2, in the respective parameter pde shows that its mixed type is reflected in the error structure of the iterative solutions. The parabolic line in Figure 1 is clearly observable in Figure 13, but also the two parabolic lines bordering the hyperbolic ring in Figure 2 are indicated in Figure 14. Especially the parabolic points lying on $\partial\Omega$ are highlighted: while in the simply supported example the iterates stay with the initial value of E_0 at the parabolic midpoints of each side of the frame and exactly reach the solution at the very corners, the parameters are left completely unchanged at the parabolic corners in the clamped case.

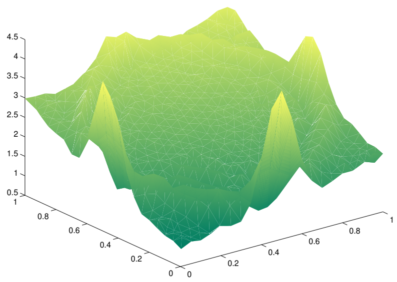

Figure 11: E_{69}, simply supported example

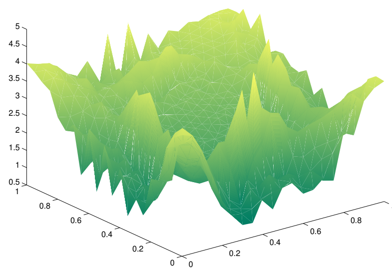

Figure 12: E_{69}, clamped example

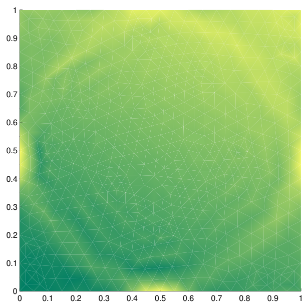

Figure 13: E_{69}, top view, simply supported

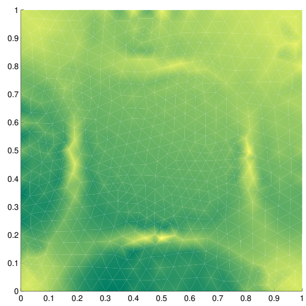

Figure 14: E_{69}, top view, clamped

From the discussion of the direct approach in Section 3 we know that the second derivatives of any solution of the direct problem, i.e., especially w_{kxx}, w_{kyy} and w_{kxy}, vanish at the parabolic boundary points - both in the simply supported and the clamped situation. Hence, the right-hand side in (4.52) is zero at these points such that the initial guess E_0 cannot change there, explaining the behaviour shown in Figures 11 and 12 along $\partial\Omega$. For that reason, these results cannot be improved by choosing a finer grid when staying with (4.52), on the contrary the peaks would even get sharper. Concerning the interior of Ω, the parabolic lines for w_k are not fixed but tend during the iteration towards those of the target $\hat{w}$ as shown in Figures 1 and 2. Hence, their influence on (4.52) is not as strong as that of the non-changing parabolic boundary points, which is also reflected in Figures 11 and 12.

We summarize our observations by

$$\bar{E}_k \approx 0 \Leftrightarrow \bar{\Delta} = 0,$$

where $\bar{\Delta}$ is the discriminant of the parameter pde (3.35), finally suggesting that the parameter cannot be identified along the parabolic lines determined by $\bar{\Delta} = 0$. This lack of identifiability does also exist during the iteration based on update (4.44), (4.45) but then is blurred out due to the smoothing effect of the pde for $\bar{E}_k$.

Considering the direct approach for solving the inverse problem via the second order pde (3.35), the question if or what kind of boundary conditions on E should be prescribed is unanswered. This automatically translates into an uncertainty about "the right inner product" for the left-hand side in (4.43). However, as opposed to the direct approach, the iterative process allows at least to test several choices. So far, we considered two possibilities, namely the neglect of boundary conditions via (4.52) and the prescription of Neumann data via (4.45). Aiming at a smooth approximation of the parameter - regarding the motivating sag bending process only then suitable for a translation into a heating procedure -, the latter variant is certainly to prefer. If the boundary values of the solution (or the desired) E_* are given, we could use this information by a further manipulation of the iterative process (4.42). Restricting the test functions h in (4.43) from the space $H^1(\Omega)$ to $H_0^1(\Omega)$, we again can interpret (4.43) as the weak formulation of the elliptic pde (4.44) for the update $\bar{E}_k$ but now with

$$\bar{E}_k = 0 \quad \text{on} \quad \partial\Omega \tag{4.54}$$

as boundary condition. Then, the Dirichlet trace of the initial guess E_0 are maintained during the iteration. In terms of formulation (3.20), (4.44) in combination with (4.54) can be understood as building the adjoint of the iteration operator with respect to $H_0^1(\Omega)$.

The course of the iteration using (4.54) with an initial guess

$$E_0 = E_* + \frac{3}{2}\sin(\pi x)\sin(\pi y)$$

is recorded in Figures 15 and 16. The relative errors in the parameter and the output

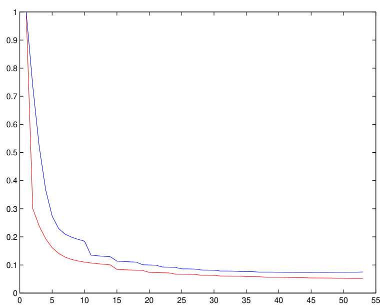

Figure 15: (4.50) vs. k

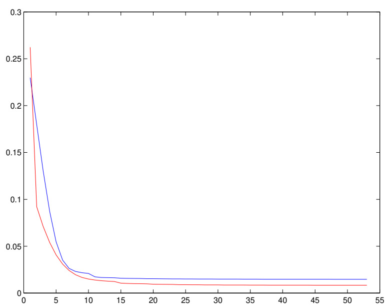

Figure 16: (4.51) vs. k

now are nearly identical in the simply supported (red line) and the clamped situation (blue line), furthermore they are (of course) below their counterparts from Figures 3 and

4. Nevertheless, the difference between the simply supported and the clamped example becomes apparent when regarding the absolute error between E_* and the respectively computed parameters E_{53} from the top as illustrated in Figures 17 and 18. Once again,

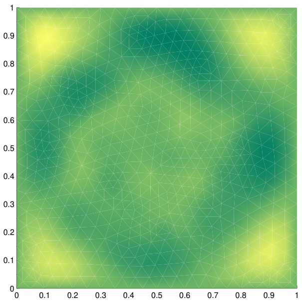

Figure 17: $E_* - E_{53}$, simply supported, top view

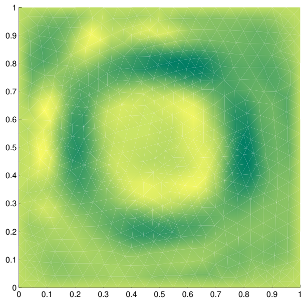

Figure 18: $E_* - E_{53}$, clamped, top view

the structure of the mixed type parameter pde (3.35) is reflected in the results obtained by the iterative parameter identification method.

Finally, we briefly comment on the influence of data perturbations on the inverse windshield problem. Staying with the update rule (4.54), which led to the best results in the noise free situation, we now consider random perturbations w_C^δ and w_S^δ of the exact data (4.46) and (4.47). The respective relative data errors are given in Table 1. Though the

	δ	$\frac{\|\|w^\delta - \hat{w}\|\|}{\|\|\hat{w}\|\|}$	$\frac{\|\|w^\delta - \hat{w}\|\|_{H^1(\Omega)}}{\|\|\hat{w}\|\|_{H^1(\Omega)}}$	$\frac{\|\|w^\delta - \hat{w}\|\|_{L^2(\Omega)}}{\|\|\hat{w}\|\|_{L^2(\Omega)}}$
$w = w_S$	0.292	0.293	0.012	0.001
$w = w_C$	0.417	0.29	0.02	0.002

Table 1: the data error

errors are about 29% when measured with respect to the full $H^2(\Omega)$-norm, they are less than half a percent if the perturbations are considered only in $L^2(\Omega)$. The numbers of the table also confirm our earlier request for approximating the given target shield (no matter if exact or perturbed) in the full $H^2(\Omega)$-norm. Only then, errors in the second order derivatives and the related curvature terms can be minimized, which is essential for the optical quality of the windshield. Figures 19 and 20 now show the behaviour that is typical for any iterative parameter identification method in the presence of data noise. While the relative error (4.51) (with $\hat{w}$ replaced by w^δ) in the output is monotonically decreasing, the error in the parameter shows a semi-convergent behaviour (even though the true boundary values were fixed). Hence, a reliable approximation of E_* can only be

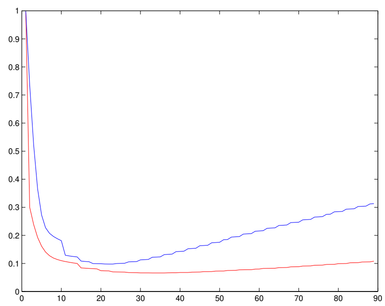

Figure 19: (4.50) vs. k

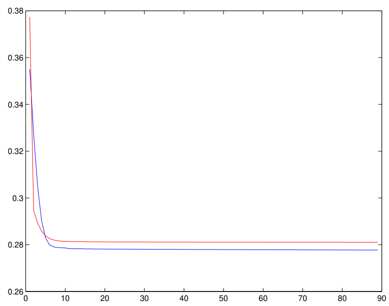

Figure 20: (4.51) vs. k

obtained by stopping the iteration at the right time, for instance according to the discrepancy principle (3.18). Furthermore, Figure 19 indicates that the iteration for the clamped case (blue line) is more sensitive to data perturbations than for the simply supported one (red line).

The theoretical and numerical results presented in this paper clearly demonstrate that the inverse windshield problem (3.14) can be solved in a stable way by the derivative free iteration method (3.20) under natural assumptions and minimal effort. Furthermore, we have seen that the direct approach, though methodologically different and (so far) not admitting a numerical implementation, is coupled to the iteration. A better understanding of its mixed type structure is of own mathematical interest but might also help to further improve the performance of the iterative algorithm.

Acknowledgement: I'd like to express my gratitude to Prof Heinz W Engl and the group of J R Ockendon for bringing the windshield problem to my attention, and for fruitful discussions about the two approaches.

References

[1] D. Braess, Finite Elements, Cambridge University Press, 2001

[2] P.G. Ciarlet, Mathematical Elasticity. Volume I: Three-dimensional Elasticity, Studies in Mathematics and its Applications 20, North-Holland, Amsterdam, 1988 the solution of nonlinear ill-posed problems under affinely invariant conditions, Inverse Problems 14 (1998), 1081–1106

[3] H.W. Engl, M. Hanke and A. Neubauer, Regularization of Inverse Problems, Kluwer Academic Publishers, Dordrecht 1996 (Paperback edition 2000) regularization of nonlinear ill-posed problems, Inverse Problems 5 (1989), 523-540

[4] H.W. Engl, P. Kügler, The influence of the equation type on iterative parameter identification problems which are elliptic or hyperbolic in the parameter, European Journal of Applied Mathematics, to appear

[5] H.W. Engl, O. Scherzer, Convergence rate results for iterative methods for solving nonlinear ill-posed problems, in: D. Colton, H.W. Engl, A.K. Louis, J. McLaughlin, W.F. Rundell (eds.), Surveys on Solution Methods for Inverse Problems, Springer, Vienna/New York, 2000, 7-34

[6] R. Fletcher, Practical Methods of Optimization Vol. 1, John Wiley and Sons, 1980

[7] M. Hanke, A. Neubauer, O. Scherzer, A convergence analysis of the Landweber iteration for nonlinear ill-posed problems, Numerische Mathematik 72 (1995), 21–37

[8] D. Krause, H. Loch (Eds.), Mathematical Simulation in Glass Technology, Springer-Verlag Berlin Heidelberg New York, 2002

[9] P. Kügler, A Derivative Free Landweber Iteration for Parameter Identification in Elliptic Partial Differential Equations with Application to the Manufacture of Car Windshields, PhD-Thesis, Johannes Kepler Universität Linz, Austria, 2002

[10] W. Litvinov, Optimization in Elliptic Problems with Applications to Mechanics of Deformable Bodies and Fluid Mechanics, Birkhäuser Verlag, Basel, Boston, Berlin, 2001

[11] S. Manservisi, Control and optimization of the sag bending process in glass windscreen design, in: L. Arkeryd, J. Bergh, P. Brenner, R. Pettersson, Progress in Industrial Mathematics at ECMI98, Teubner, Stuttgart, 1999, 97–105

[12] O.S. Narayanaswamy, Stress and structural relaxation in tempering glass, Journal of the American Ceramic Society, 61 (1978), 146–152

[13] J. Ockendon, S. Howison, A. Lacey and A. Movchan, Applied Partial Differential Equations, Oxford University Press, 1999

[14] D. Salazar, R. Westbrook, Inverse problems of mixed type in linear plate theory, preprint

[15] E. Schock, Approximate solution of ill-posed equations: arbitrarily slow convergence vs. superconvergence, in: G. Hämmerlin and K. Hoffmann, eds., Constructive Methods for the Practical Treatment of Integral Equations, Birkhäuser, Basel 1985, 234-243

[16] D. Temple, An Inverse System - An Analysis Arising from Windscreen Manufacture, MSc Thesis, University of Oxford, England, 2002

[17] E. Zeidler, Nonlinear Functional Analysis and its Applications II/a, Springer-Verlag, New York, Berlin, Heidelberg, 1980